

## Article

# Development of V-Based Oxygen Carriers for Chemical Looping Oxidative Dehydrogenation of Propane

Tianwei Wu <sup>1,2</sup>, Qingbo Yu <sup>2</sup>, Kun Wang <sup>1,2</sup> and Martin van Sint Annaland <sup>1,\*</sup>

<sup>1</sup> Chemical Process Intensification, Department of Chemical Engineering and Chemistry, Eindhoven University of Technology, P.O. Box 513, 5600 MB Eindhoven, The Netherlands; wtwneu@163.com (T.W.); wangkun@mail.neu.edu.cn (K.W.)

<sup>2</sup> School of Metallurgy, Northeastern University, No. 11, Lane 3, Wenhua Road, Heping District, Shenyang 110819, China; yuqb@smm.neu.edu.cn

\* Correspondence: m.v.sintannaland@tue.nl; Tel.: +31-40-247-2241

**Abstract:** Two different preparation methods, viz. incipient impregnation and mechanical mixing, have been used to prepare V-based oxygen carriers with different V loadings for chemical looping oxidative dehydrogenation of propane. The effect of the preparation method, V loading, and reaction temperature on the performance of these oxygen carriers have been measured and discussed. It was found that the VO<sub>x</sub> species can be well distributed on the support when the V loading is low (5 wt.% and 10 wt.%), but they may become aggregated at higher loadings. For oxygen carriers with a higher V loading, the oxygen transport capacity of the oxygen carrier, propane conversion and CO<sub>x</sub> selectivities increase, while the propylene selectivity decreases. With a V-loading of 10 wt.%, the maximum propylene yield was achieved. The VO<sub>x</sub> species were better distributed over the support when applying the impregnation method; however, at higher V loadings the V-based oxygen carriers prepared by mechanical mixing showed a larger oxygen transport capacity. The oxygen carriers prepared by impregnation showed a better performance for the oxidative dehydrogenation of propane (ODHP) and re-oxidation reactions compared to oxygen carriers prepared by mechanical mixing. Higher reaction temperatures are favorable for the re-oxidation reaction, but unfavorable for the propylene production.

**Keywords:** chemical looping; oxidative dehydrogenation of propane; V-based oxygen carrier; loading; preparation method



**Citation:** Wu, T.; Yu, Q.; Wang, K.; van Sint Annaland, M. Development of V-Based Oxygen Carriers for Chemical Looping Oxidative Dehydrogenation of Propane. *Catalysts* **2021**, *11*, 119. <https://doi.org/10.3390/catal11010119>

Received: 24 December 2020

Accepted: 7 January 2021

Published: 15 January 2021

**Publisher's Note:** MDPI stays neutral with regard to jurisdictional claims in published maps and institutional affiliations.



**Copyright:** © 2021 by the authors. Licensee MDPI, Basel, Switzerland. This article is an open access article distributed under the terms and conditions of the Creative Commons Attribution (CC BY) license (<https://creativecommons.org/licenses/by/4.0/>).

## 1. Introduction

Propylene is one of the most important intermediate chemicals and is used for the production of many important materials, such as polypropylene, propylene oxide and acrylonitrile [1]. Because of the rapid increase in the demand for propylene-derived products, global propylene demand keeps growing in recent years. Nowadays, the development of the shale gas industry has increased the availability of low-cost propane, which makes the production of propylene from propane more and more attractive [2]. The predominant process for propylene production from propane is the catalytic dehydrogenation of propane, by which propane is directly dehydrogenated in the presence of a catalyst at relatively high temperatures. However, the main reaction of this process is a typical endothermic reaction, which makes this process carbon and energy intensive [3]. Moreover, the thermodynamic equilibrium limitation of the main reaction limits the maximum propylene yield [4]. In addition, at high temperatures, undesired cracking side reactions will be very difficult to avoid, which leads to rapid coke formation, thereby deactivating the catalyst [5]. These inherent disadvantages limit the performance of the catalytic dehydrogenation of propane.

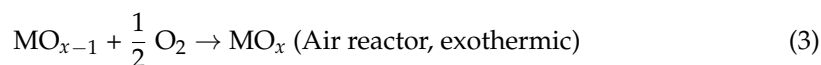
The oxidative dehydrogenation of propane (ODHP) for the production of propylene has been explored to replace the catalytic dehydrogenation of propane [6]. In this process propane and gaseous oxygen are co-fed to a catalyst, where the gaseous oxygen is used to

combust the hydrogen by-product, which removes the equilibrium limitation and renders the overall process exothermic ( $\Delta H = -139.95$  kJ/mol at 400 °C):



In recent decades, a lot of research has been focused on ODHP for the development of a suitable catalyst, the investigation of the reaction mechanism and the intensification of the process [6]. High propane conversions (>30%) with satisfying propylene selectivities (>75%) have been reported in the literature; for example, with a vanadium-doped porous silica catalyst a propane conversion of 64% with a propylene selectivity of about 90% has been achieved [7–9]. Although these propane conversions and propylene selectivities are very promising, the traditional ODHP still has some inevitable disadvantages, particularly related to the safety issues associated with the formation of potentially explosive mixtures when co-feeding propane and gaseous oxygen due to the high flammability of the propane, and the high operation and investment costs for the air separation unit for the production of pure oxygen [10]. In addition, the separation of products from the product stream from a traditional ODHP reactor is intricate and energy extensive [10,11]. Because of the strong oxidizing property of gaseous oxygen, many of the shortcomings of traditional ODHP are inevitable. In order to remedy some of these shortcomings, it has been explored whether  $\text{CO}_2$  and  $\text{N}_2\text{O}$  as weaker oxidants can replace the gaseous oxygen to partially oxidize propane to propylene [12,13]. However, these oxidants have their own limitations, such as their high price as feedstock, and downstream separation.

In order to overcome the shortcomings of these propylene production technologies, a new propylene production route has been proposed, viz., chemical looping oxidative dehydrogenation of propane (CL-ODHP), which can address the disadvantages [14]. In CL-ODHP, the active phase of an oxygen carrier donates its lattice oxygen to convert propane to propylene and water, during which the active phase of the oxygen carrier is reduced. Subsequently, the reduced oxygen carrier will be transferred to the air reactor, where the missing lattice oxygen of the active phase is re-supplied by the air. After, the re-oxidized oxygen carrier is transported back to the ODHP reactor, completing the chemical loop. Thus, the oxygen can be transported from the air reactor to the ODHP reactor by repeated reduction and oxidation of the oxygen carrier. The reactions in the two reactors can be represented as follows:



The process of CL-ODHP has several inherent advantages over other propylene production technologies: (a) decrease in the dehydrogenation and downstream separation energy consumption by oxidation of the hydrogen; (b) reduction in investment and operating costs by eliminating air separation units; (c) reduction/circumvention of explosion hazards of propane; (d) increase in operability and temperature control by carrying out the reactions in the absence of gaseous oxygen [15,16]; (e) reduction of  $\text{CO}_2$  and  $\text{NO}_x$  emissions by indirect flameless combustion of hydrogen [17].

As a chemical looping application, the development of a suitable oxygen carrier is of paramount importance for CL-ODHP. However, compared to the catalysts used in traditional ODHP and the oxygen carriers for other chemical looping applications, the development of oxygen carriers for the CL-ODHP process has received much less attention. For the development of oxygen carriers for the CL-ODHP process, the development of catalysts for the traditional ODHP process and oxygen carriers for other chemical looping applications can serve as a reference, and a short overview is given below.

Supported catalysts and oxygen carriers have proven their good performance in traditional ODHP and chemical looping technologies [18,19]. As the V-based supported

catalyst combines a good catalytic activity with environmental-friendly properties, it has been widely used in research into traditional ODHP [20,21]. Ovsitser et al. prepared a supported V-based catalyst, which showed stable performance and satisfying propylene yield under oxygen-lean conditions [8]. Hu et al. prepared a novel supported V-based catalyst for the oxidative dehydrogenation of propane by loading the  $\text{VO}_x$  to porous silica materials, and this catalyst showed a superior propane conversion and stable propylene selectivity [7]. In chemical looping technologies, the supported oxygen carriers also showed good reactivity and stability. Jose et al. reported a supported Ni-based oxygen carrier for low temperature chemical looping applications, and this oxygen carrier showed promising behavior and sufficient reaction kinetics [22]. Wang et al. used mechanical mixing to prepare the Cu-based oxygen carrier for chemical looping air separation, where the support was used to effectively prevent agglomeration of the oxygen carrier particles, and this oxygen carrier exhibited a high reactivity and stability during multi-cycle tests [23]. For supported catalysts and oxygen carriers, commonly used supports include  $\text{SiO}_2$ ,  $\text{Al}_2\text{O}_3$ ,  $\text{TiO}_2$ ,  $\text{ZrO}_2$ , and  $\text{MgO}$  [6,18]. Among these oxygen carriers,  $\text{Al}_2\text{O}_3$  is the most commonly used support because of its good pore structure, large specific surface area, suitable surface properties, excellent thermal stability and mechanical strength [18,24].

The common preparation methods for supported oxygen carriers include impregnation, sol-gel and mechanical mixing [25–28]. It has been demonstrated that the preparation method can have a great influence on the final physical and chemical properties, like specific surface area, pore structure and size, oxygen transport capacity, active phase distribution, and reaction reactivity [25]. Therefore, it is necessary to understand the effect of different preparation methods on the physical and chemical properties for a novel oxygen carrier and determine the best preparation method. Besides the preparation method, the active phase loading on the support has a big impact on the physical and chemical properties of the supported oxygen carriers [29,30]. Too high or too low loadings will be unfavorable for the performance of the oxygen carrier. At low loadings, the mechanical strength and the oxygen storage capacity of the oxygen carrier limit their effective use for chemical looping applications [24,30], whereas at high loadings, significant agglomeration of the active phase can occur which tends to promote undesired side reactions, thereby decreasing the selectivity of the target product [30]. In addition, high loadings of the active phase could reduce the thermal stability and oxygen storage capacity of the oxygen carrier in comparison to the optimal loading [23,30,31]. Therefore, it is important to determine the optimal active phase loading for optimal performance of a specific oxygen carrier. Although superior catalytic performance of  $\text{VO}_x$  species in the catalysts for the traditional ODHP process have been reported, the reactivity performance of  $\text{VO}_x$  species as the active phase of oxygen carriers for CL-ODHP remains to be studied.

The aim of this work is the investigation of the effect of the active phase loading and the oxygen carrier preparation method on the performance of V-based oxygen carriers for CL-ODHP, and to study the effect of reaction temperature on both the oxidative dehydrogenation reaction of propane and the re-oxidation reaction of the reduced oxygen carrier for V-based oxygen carriers. Two different commonly applied oxygen carrier preparation methods, viz. the impregnation method and mechanical mixing method, have been used to prepare a series of oxygen carriers with different V loadings (5 wt.%, 10 wt.%, 15 wt.% and 20 wt.%). The physical and chemical properties of the thus prepared oxygen carriers were characterized by state-of-the-art characterization methods, and the reactivity performance of these oxygen carriers for both propane oxidative dehydrogenation and the re-oxidation of the reduced oxygen carrier was investigated with a micro fixed bed reactor.

## 2. Results and Discussions

### 2.1. Characterization of the Oxygen Carriers

First the prepared oxygen carriers were characterized with  $\text{N}_2$  adsorption, X-ray diffraction (XRD) and SEM-EDX (scanning electron microscope and energy dispersive spectrometry). The determined Brunauer-Emmett-Teller (BET) surface areas of the as-

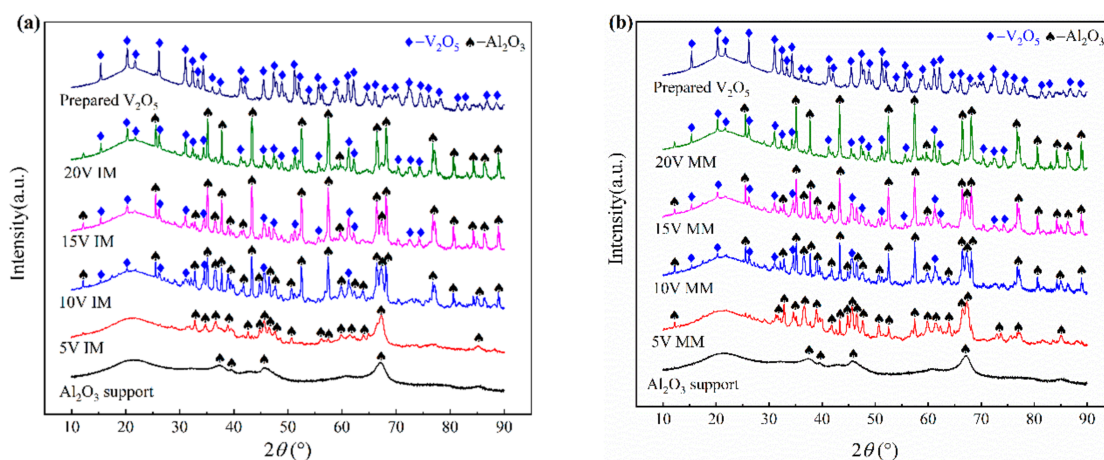
prepared oxygen carriers are listed in Table 1. When the V loading is increased from 5 wt.% to 20 wt.%, the surface areas of the V-based oxygen carriers prepared by impregnation and mechanical mixing decrease from 30.96 m<sup>2</sup>/g to 0.46 m<sup>2</sup>/g and 4.43 m<sup>2</sup>/g to 0.29 m<sup>2</sup>/g, respectively. The decrease in the surface areas with increasing V loadings implies that the VO<sub>x</sub> species enter the pore channels of the Al<sub>2</sub>O<sub>3</sub> support or partially destroy the framework of the support during the high temperature calcination [32,33]. The specific surface areas of the V-based oxygen carriers prepared by impregnation are larger than those prepared by mechanical mixing, which indicates a better distribution of the VO<sub>x</sub> species over the support when using the impregnation method. When comparing the surface areas of the V-based oxygen carriers to other supported V-based catalysts reported in the literature, the surface area is relatively low. However, the measured surface areas are typical for oxygen carriers used in chemical looping applications [10,34–36]. Typically a lower surface area can be accepted for oxygen carriers, since the oxygen activity of oxygen carriers depends more on the internal oxygen transport rate in the grains than the surface area [10,36].

**Table 1.** The BET surface area and quantitative results of thermogravimetric (TGA) analysis.

Oxygen Carrier	Brunauer-Emmett-Teller (BET) Surface Area (m <sup>2</sup> /g)	Reduction Peak(s) Temperature (°C)	Oxidation Peak(s) Temperature (°C)	Average Weight Change (mg)
5V IM	30.96	545.5	373.4	0.3965
10V IM	1.92	615.0	378.4 448.1	0.8155
15V IM	1.54	647.4	394.4 513.4	1.0698
20V IM	0.46	594.4 613.9 642.9	395.4 516.9	1.4469
5V MM	4.43	561.6	409.4	0.3829
10V MM	1.59	622.4	404.4 482.4	0.8103
15V MM	1.04	636.4 651.5	396.1 500.6	1.1899
20V MM	0.29	622.4 647.9 673.4	411.9 528.6	1.5628

Figure 1 shows the XRD patterns of the prepared oxygen carriers with different V loadings and preparation methods. The patterns of the Al<sub>2</sub>O<sub>3</sub> support and V<sub>2</sub>O<sub>5</sub> are also shown in Figure 1. The amorphous Al<sub>2</sub>O<sub>3</sub> support shows broad peaks in the XRD pattern [7], but after vanadium loading the peaks of alumina become sharper, indicating an increase in the crystallinity. No significant diffraction peaks of VO<sub>x</sub> species can be observed when the V loading is low (5 wt.%) indicating that the vanadium oxide species are dispersed well on the Al<sub>2</sub>O<sub>3</sub> support, or alternatively their grain sizes are small in the case of low V loading, so that they cannot be detected by XRD [12,37]. When the V loading increases to 10 wt.%, some small peaks of V<sub>2</sub>O<sub>5</sub> can be seen in the XRD patterns, implying that the V<sub>2</sub>O<sub>5</sub> starts to become more aggregated on the Al<sub>2</sub>O<sub>3</sub> support. With a further increase in the V loading, the peaks of the VO<sub>x</sub> species become more and more pronounced. For the 15V IM, 15V MM, 20V IM and 20V MM samples, the obvious peaks of V<sub>2</sub>O<sub>5</sub> can be seen in the patterns, corresponding to the increased aggregation of VO<sub>x</sub> species on the Al<sub>2</sub>O<sub>3</sub> support at higher loadings [7]. Meanwhile, the peaks of chemical compounds of the VO<sub>x</sub> and Al<sub>2</sub>O<sub>3</sub> support cannot be observed in the XRD patterns of all oxygen carriers

shown in Figure 1, which indicates that the  $V_2O_5$  does not react with  $Al_2O_3$  support during the preparation with different methods and at different V loading.



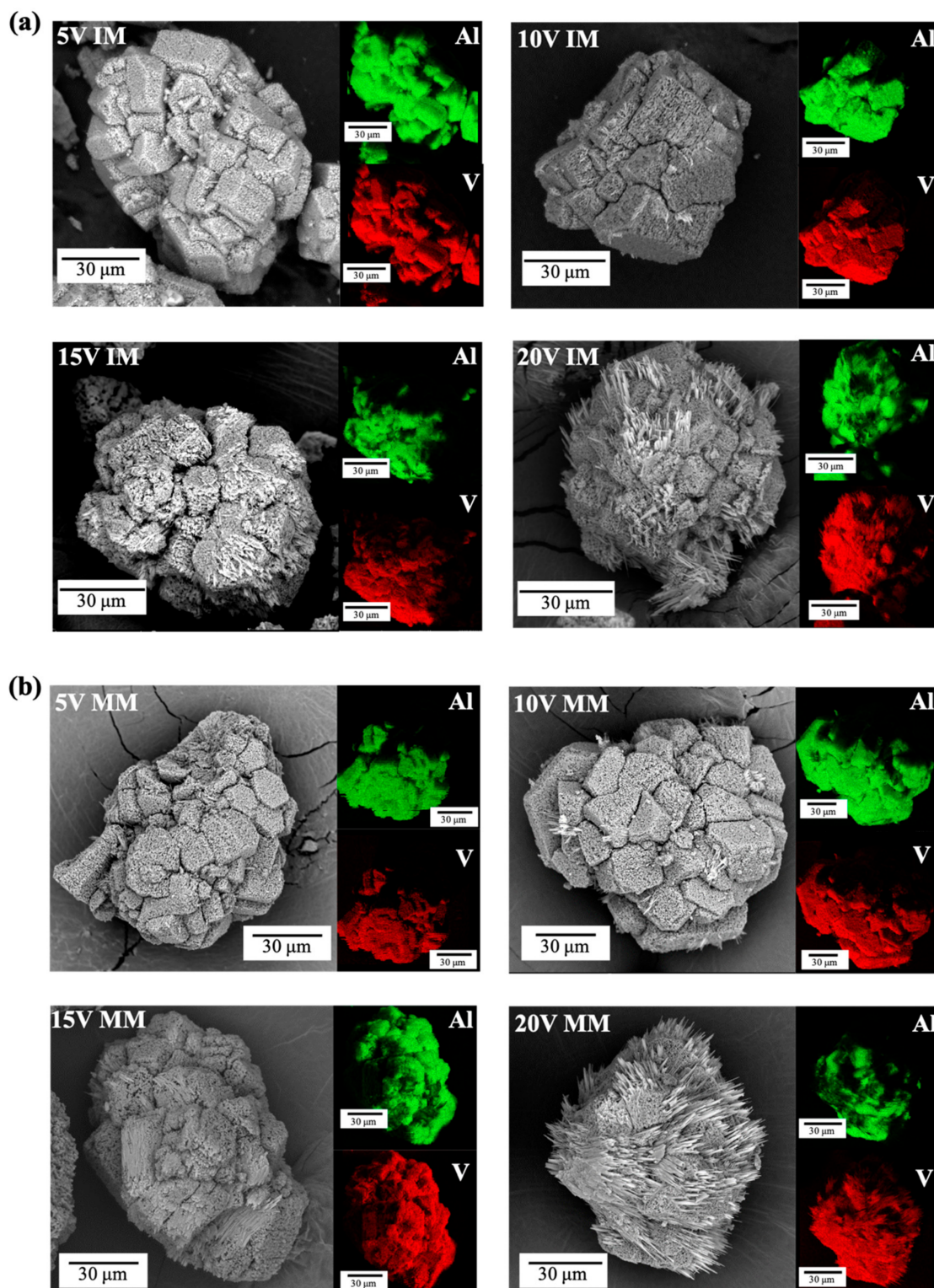
**Figure 1.** The X-ray diffraction (XRD) patterns of V-based oxygen carriers with different V loadings,  $Al_2O_3$  support and prepared  $V_2O_5$ : (a) Impregnation method; (b) Mechanical mixing method.

Figure 2 illustrates the morphologies and element distribution maps of the as-prepared V-based oxygen carriers investigated by SEM-EDX. For 5V IM and 5V MM, no crystal phase morphologies of  $VO_x$  species can be seen on the SEM image of the oxygen carrier particle surfaces, as well as no rich or lean regions of V and Al in the EDX element distribution maps, which indicates that the V and Al are distributed well over the particle surface. For 10V IM and 10V MM, a small number of needle-like phase morphologies can be seen on the particle surface and these are attributed to  $VO_x$  species [38,39]. This means that  $VO_x$  species begin to aggregate on the particle surface when the V loading is at around 10 wt.%. However, from the element distribution maps, it can be seen that the Al and V are still well distributed over the particle surface at 10 wt.% V loading. When the V loading increases to 15 wt.% and 20 wt.%, more needle-like  $VO_x$  species can be discerned on the oxygen carrier particle surface, showing that the  $VO_x$  species become more and more aggregated on the  $Al_2O_3$  support at such high loadings. Moreover, at these high V loadings (15 wt.% and 20 wt.%) distinct regions lean in Al and rich in V can be observed in the element distribution maps, also indicating aggregation of the  $VO_x$  species at such high V loadings. The results of the SEM-EDX are in good correspondence with the XRD results, indicating that the  $VO_x$  species is well distributed over the support when the V loading is kept below 10 wt.%.

## 2.2. Redox Performance of Oxygen Carriers

To determine the effects of different V loadings and preparation methods on the redox properties of prepared V-based oxygen carriers, the  $H_2$ -TPR,  $O_2$ -TPO and isothermal redox cycles were implemented by the TGA. The results are shown in Figure 3 and Table 1. From Figure 3a, it can be seen that for 5V IM, 10V IM and 15V IM, there is only one obvious reduction peak in the  $H_2$ -TPR patterns. This reduction peak is ascribed to well-dispersed  $VO_x$  species [7,32]. When the V loading increases from 5 wt.% to 15 wt.%, the reduction peak temperature rises from 545.5 °C to 647.4 °C, which suggests that the well-dispersed  $VO_x$  species become increasingly more aggregated on the particle surface thereby retarding their reduction [40]. For the 20V IM sample, three reduction peaks can be observed, implying the presence of bulk  $V_2O_5$  at 20 wt.% V loading, corresponding to the three step reduction of  $V_2O_5$ :  $V_2O_5 \rightarrow V_6O_{13} \rightarrow V_2O_4 \rightarrow V_2O_3$  [41]. When comparing Figure 3a with Figure 3c, it can be observed that the reduction peak(s) temperatures of V-based oxygen carriers prepared by the mechanical mixing method are higher than those prepared by the impregnation method for each V loading. The results of the  $H_2$ -TPR further indicate

that the  $\text{VO}_x$  species can be distributed well when the V loading is relatively low and that with the impregnation method the  $\text{VO}_x$  species are better distributed on the  $\text{Al}_2\text{O}_3$  support compared to the mechanical mixing method.



**Figure 2.** Morphologies and element distribution maps of V-based oxygen carriers with different V loadings: (a) Impregnation method; (b) Mechanical mixing method.

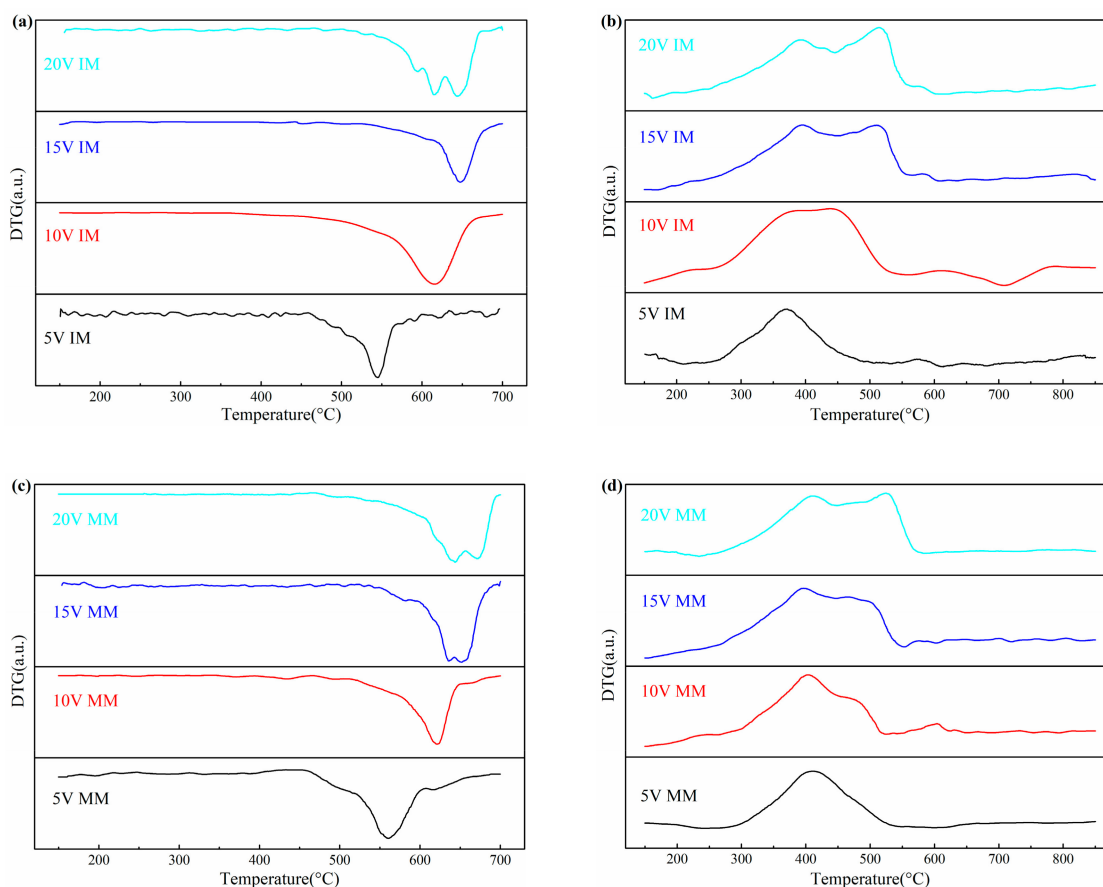


**Figure 3.** H<sub>2</sub>-TPR and O<sub>2</sub>-TPO profiles for V-based oxygen carriers with different V loadings: (a) H<sub>2</sub>-TPR for impregnation method, (b) O<sub>2</sub>-TPO for impregnation method, (c) H<sub>2</sub>-TPR for mechanical mixing method, (d) O<sub>2</sub>-TPO for mechanical mixing method.

Figure 3b shows the O<sub>2</sub>-TPO patterns of different V-based oxygen carriers prepared by impregnation. As shown in Figure 3b, there is only one oxidation peak for 5V IM, and when the V loading is increased, the oxidation peak of the reduced V-based oxygen carriers first becomes wider (for 10V IM) and then separates into two oxidation peaks (for 15V IM and 20V IM). The two oxidation peaks of V-based oxygen carriers at higher V loading indicate a multi-step oxidation. In addition, with increasing V loading, the oxidation peaks of the V-based oxygen carriers shift to higher temperatures. When comparing Figure 3b with Figure 3d, it can be found that the oxidation peak(s) temperatures of reduced V-based oxygen carriers prepared by impregnation are somewhat lower than those prepared by mechanical mixing for each V loading, corresponding to the better distribution of the VO<sub>x</sub> species, facilitating their re-oxidation.

Figure 4 shows the results of the isothermal redox cycles for the V-based oxygen carriers prepared with different V loadings and by different preparation methods. It can be seen from Figure 4 that the total weight changes of all the prepared oxygen carriers hardly change over five redox cycles, implying that all the prepared V-based oxygen carriers show a good redox stability. For the 5V IM and 5V MM, the weight changes are almost identical, but when the V loading is increased, the difference in the weight changes for the V-based oxygen carriers prepared by the two different methods become slightly larger. The V-based oxygen carriers prepared by impregnation show smaller weight changes during the redox cycles than those prepared by mechanical mixing, from which it can be concluded that the V-based oxygen carriers prepared by mechanical mixing can donate more lattice oxygen at high V loadings.

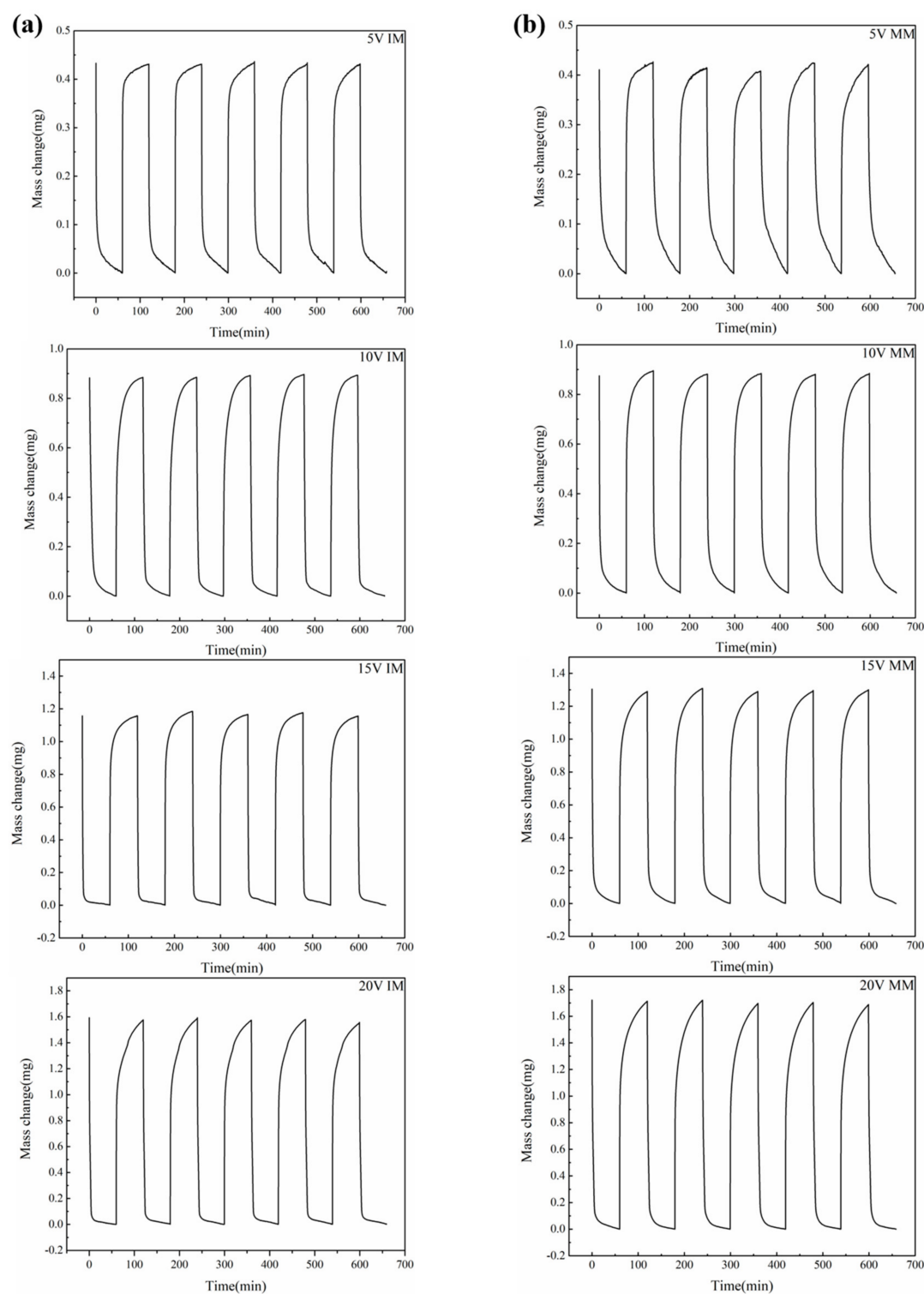


**Figure 4.** Isothermal redox cycles profiles for V-based oxygen carriers with different V loadings and preparation methods: (a) Impregnation method, (b) Mechanical method.

### 2.3. Reactivity Performance of Oxygen Carriers

#### 2.3.1. Effect of Loading

Figure 5 shows the ODHP reaction performance at 615 °C for V-based oxygen carriers with different V loadings prepared by impregnation. Figure 5 shows that for the studied V-

based oxygen carriers the initial propane conversions and  $\text{CO}_x$  selectivities are the highest and decrease with time, while the initial propylene selectivities are initially the lowest and increase with time. The decrease in the propane conversions and  $\text{CO}_x$  selectivities is mainly due to the consumption of lattice oxygen in the V-based oxygen carriers. Moreover, at the initial stage of the ODHP reaction, there are non-selective surface oxygen species on the surface of the V-based oxygen carriers formed by the weakly bounded lattice oxygen and adsorbed oxygen during the re-oxidation reaction. Those non-selective surface oxygen species can promote over-oxidation reactions and convert propane and propylene to  $\text{CO}_x$  [42,43]. Those non-selective surface oxygen species will be consumed when reaction proceeds, thus causing the propylene selectivities to increase with time.

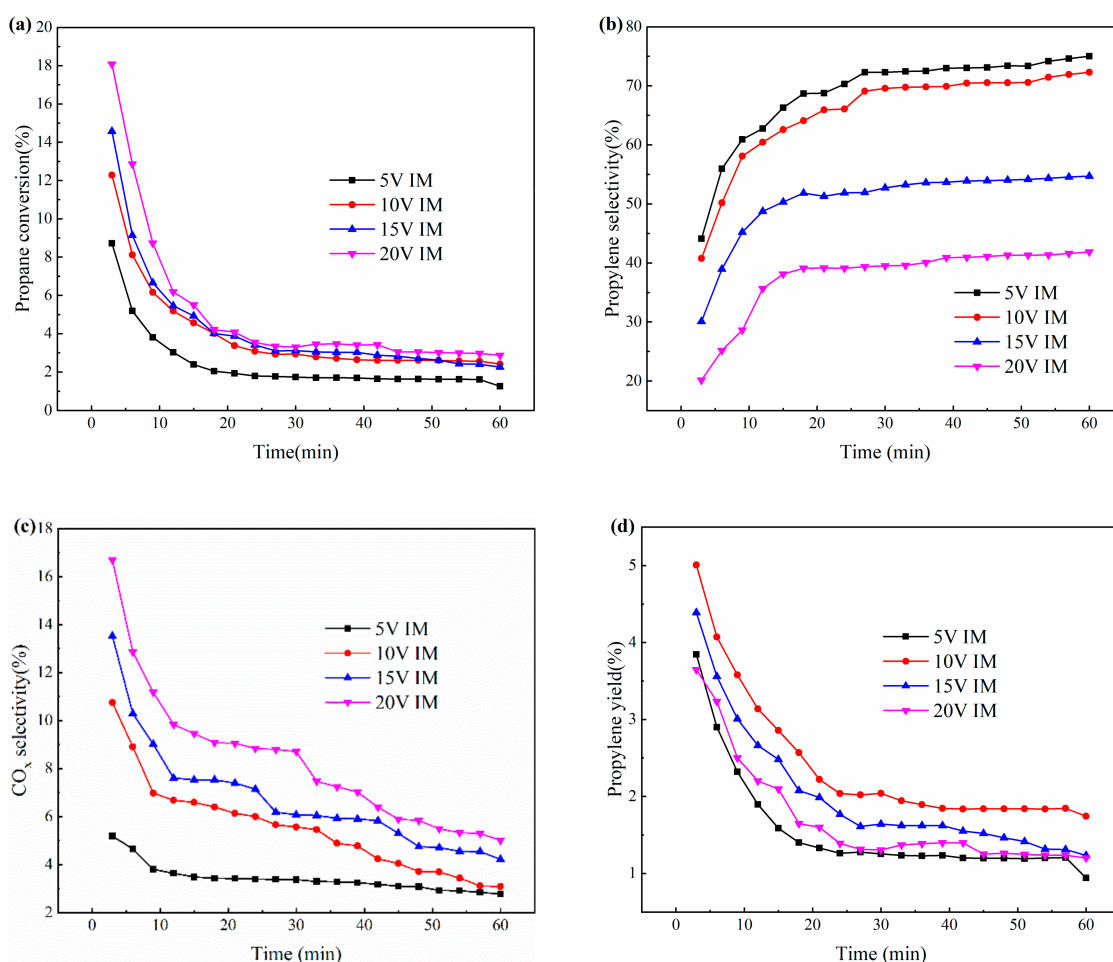


**Figure 5.** The oxidative dehydrogenation of propane (ODHP) reaction performance for V-based oxygen carriers with different V loadings by impregnation method at 615 °C: (a) Propane conversion, (b) Propylene selectivity, (c)  $\text{CO}_x$  selectivity, (d) propylene yield.

In addition, it can be seen from Figure 5 that the propane conversions increase with the V loading, while the propylene selectivities decrease and the  $\text{CO}_x$  selectivities increase (see Figure 5b,c). Oxygen carriers with a higher V loading can donate more lattice oxygen to oxidize propane. The more lattice oxygen that can be used in the ODHP reaction, the more propane can be converted, and thus the higher propane conversion that can be reached. However, the lattice oxygen can also promote the over-oxidation of propane and propylene to form  $\text{CO}_x$ . At higher V loadings, the propane is converted more to  $\text{CO}_x$ , so that the propylene selectivity is decreased, and the  $\text{CO}_x$  selectivity increased. Concluding, the optimal propylene yield is achieved with a V loading of approximately 10 wt.% (see Figure 5d). For the V-based oxygen carriers with different V loadings prepared by the

mechanical mixing method, the ODHP reactivity performance with V loading and time show the same tendency as the oxygen carriers prepared by impregnation.

Figure 6 shows the re-oxidation performance at 435 °C of the V-based oxygen carriers with different V loadings prepared by the impregnation method, where the insert picture shows the average reaction rate when the conversion of the V-based oxygen carrier reaches 0.9. After the complete reduction, the reduced V-based oxygen carriers are exposed to air for re-oxidation. At the initial stage of the re-oxidation, the outlet oxygen concentrations of the studied oxygen carriers are all at a low level, implying the rapid adsorption of oxygen [23]. The initial outlet oxygen concentrations are all near the equilibrium oxygen concentrations at 615 °C, meaning that the reduced V-based oxygen carriers can be easily and fully re-oxidized by air. Moreover, as the V loading is increased, the amount of oxygen needed by the reduced oxygen carrier increases while the reaction rate decreases. For high V loadings, there are more and more aggregated reduced  $\text{VO}_x$  species in the reduced oxygen carrier, thus requiring more oxygen and more time to fully re-oxidize the reduced oxygen carrier.

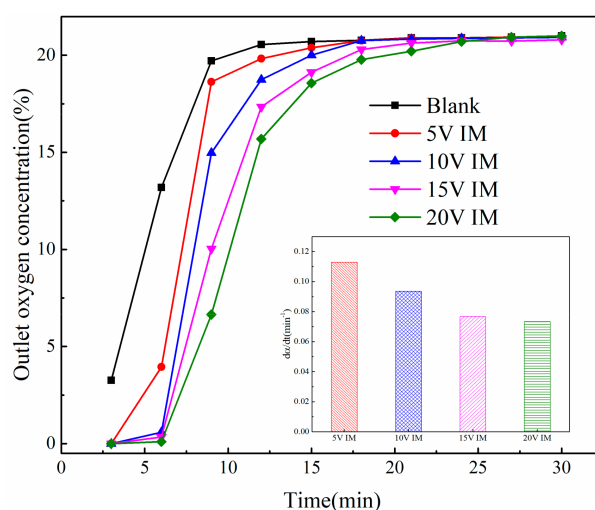


**Figure 6.** The re-oxidation performance of V-based oxygen carriers with different V loadings prepared by the impregnation method at 435 °C.

### 2.3.2. Effect of Preparation Method

Figure 7 shows the ODHP reaction performance for 10V IM and 10V MM at 615 °C. At the initial stage of the ODHP reaction, the 10V IM shows a lower propane conversion (12.82%) and  $\text{CO}_x$  selectivity (10.76%) than the 10V MM (25.13% propane conversion and 24.34%  $\text{CO}_x$  selectivity), but it also shows a much higher propylene selectivity (40.76%) than the 10V MM (14.19%). Thus, the 10V IM shows a higher propylene yield (5.01%) than 10V MM (3.57%). After 60 min, as the lattice oxygen are consumed, the propane conversions (2.41% for IM and 0.94% for 10V MM) and  $\text{CO}_x$  selectivities (3.09% for 10V IM and 10.93% for 10V MM) of the two oxygen carriers are all lower than at the initial stage, whereas the propylene selectivities (72.28% for 10V IM and 37.58% for 10V MM) have increased. At that time, the propane conversion and propylene selectivity of the 10V IM are higher than the 10V MM, while the  $\text{CO}_x$  selectivity is still lower than the 10V MM, which makes the propylene yield of the 10V IM (1.74%) higher than 10V MM (0.35%). For the oxygen carriers with other V loadings, the result of the ODHP reaction performance shows the same trend. Therefore, The V-based oxygen carriers prepared by the impregnation method outperform those prepared by the mechanical mixing method. Table 2 shows a comparison of the performance of different V-based oxygen carriers and catalysts; the single-pass maximum propylene yield is about 5% in this paper, and it can be further

improved by controlling the reaction conditions and further development of the oxygen carriers, to suit the industrial process [44–48].

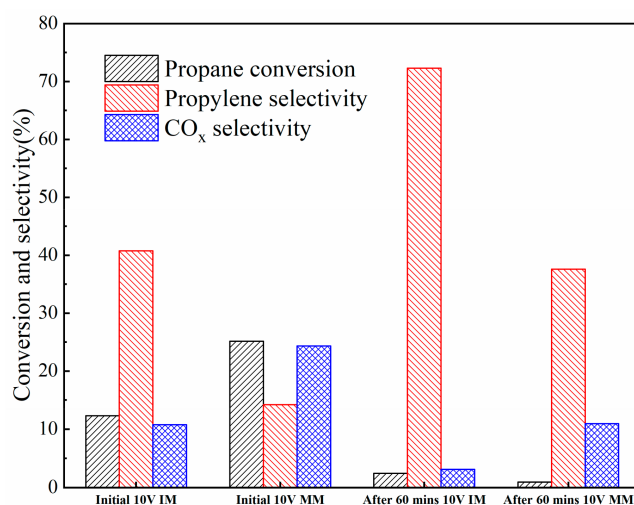


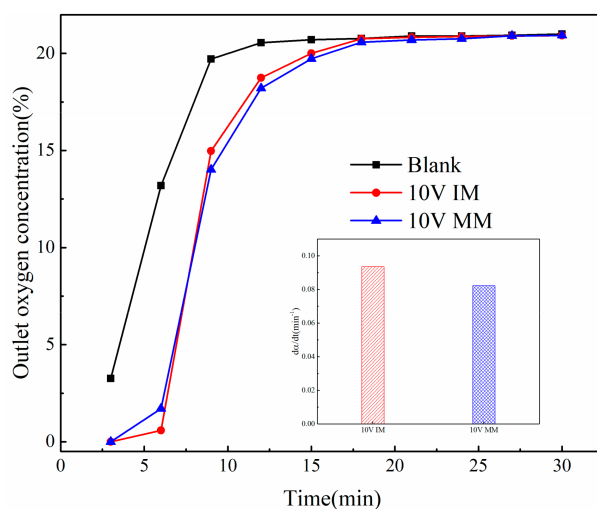
Figure 7. The ODHP reaction performance for 10V IM and 10V MM at 615 °C.

Table 2. The comparison of different V-based oxygen carriers/catalysts.

Oxygen Carrier/Catalysts	Reaction Temperature (°C)	C <sub>3</sub> H <sub>8</sub> Conversion (%)	C <sub>3</sub> H <sub>6</sub> Selectivity (%)	C <sub>3</sub> H <sub>6</sub> Yield (%)	TON <sup>a</sup>	Ref.
10V IM	615	12.82	40.76	5.01	3.36	This work
10V MM	615	25.13	14.19	3.57	2.43	This work
10% VO <sub>x</sub> /γ-Al <sub>2</sub> O <sub>3</sub>	550	6.16	60.64	3.74	1.68	[44]
V(1.0)-PEG25	450	1.4	90.0	1.2	0.767	[45]
V-Graphene	500	4.98	92.45	4.60	6.28	[49]
7.5%V/γ-Al <sub>2</sub> O <sub>3</sub>	500	25.7	89.3	22.9	13.73	[50]
7.5%V/ZrO <sub>2</sub> -γ-Al <sub>2</sub> O <sub>3</sub>	550	24.8	93.0	22.9	13.80	[50]

<sup>a</sup> TON = mole of C<sub>3</sub>H<sub>6</sub>/mole of active material.

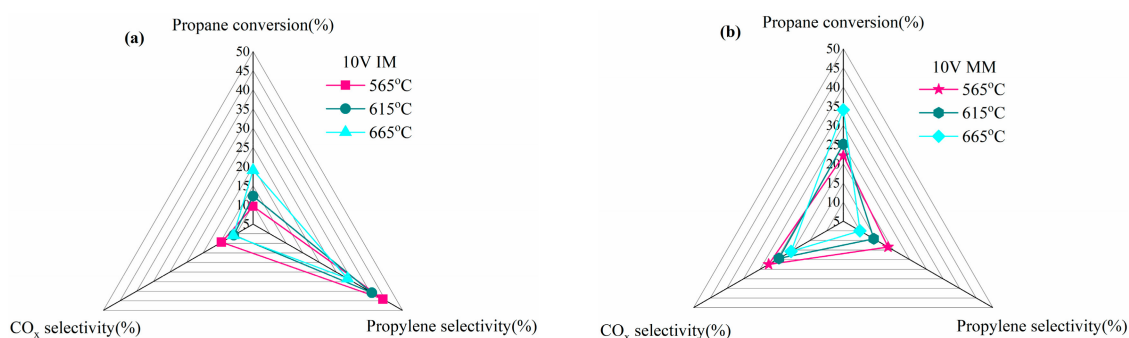
Figure 8 shows the re-oxidation performance of the V-based oxygen carriers with different preparation methods at 435 °C, where the insert picture shows the average reaction rate when the conversion of V-based oxygen carrier reaches 0.9. One can see that both V-based oxygen carriers show a low outlet oxygen concentration at the initial stage, indicating that both can adsorb the oxygen from air easily. After initial stage, the outlet oxygen concentration of 10V IM can reach 21% quickly, while the 10V MM is slightly slower. The re-oxidation reaction rate of 10V IM is slightly larger than the 10V MM as can be discerned from the insert picture in Figure 8.



**Figure 8.** The oxidation performance for 10V IM and 10V MM at 435 °C.

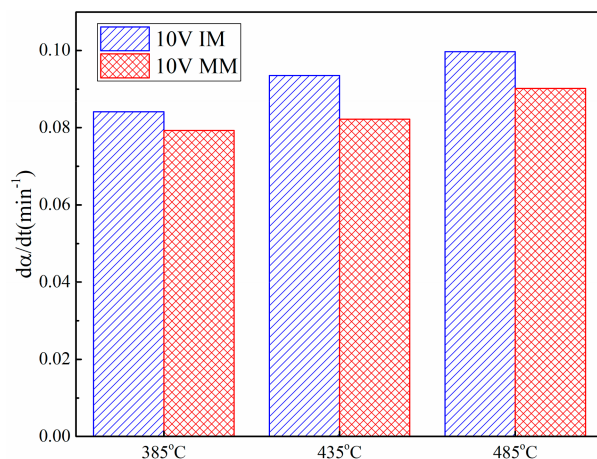
### 2.3.3. Effect of Reaction Temperature

Figure 9 shows the ODHP reaction performance of 10V IM and 10V MM at different reaction temperatures. At 565 °C, the initial propane conversions of 10V IM and 10V MM are 9.60% and 22.10%, respectively. When the reaction temperature is 665 °C, the initial propane conversions of the two V-based oxygen carriers increase to 19.02% and 34.09%, respectively. However, with the increase in reaction temperature, the initial propylene selectivities and CO<sub>x</sub> selectivities of the two V-based oxygen carriers decrease. The higher reaction rate promotes propane and propylene cracking reactions, which means more propane is converted to C<sub>1</sub>, C<sub>2</sub> and carbon, and not to propylene, and propylene is converted to these by-products. Thus, the propane conversions increase with increasing reaction temperature, but the propylene selectivity decreases. Meanwhile, as the combustion of propane and propylene are all exothermic reactions, high temperature can prevent the CO<sub>x</sub> formation, thus the CO<sub>x</sub> selectivities also decrease with the reaction temperature.



**Figure 9.** The initial ODHP performance for 10V IM and 10V MM at different temperatures (a) 10V IM, (b) 10V MM.

The conversion rate of 10V IM and 10V MM at different reaction temperatures is depicted in Figure 10, showing that the conversion rate of both V-based oxygen carriers increase with reaction temperature before the conversion reaches 0.9. The re-oxidation reaction of the V-based oxygen carrier is a temperature dependent reaction, and the oxygen concentration of the fed air (21%) is much larger than the equilibrium oxygen concentration at the studied reaction temperatures, thus the conversion rate of V-based oxygen carriers increases with increasing reaction temperature. Moreover, it can be observed that the conversion rates of the 10V IM oxygen carriers are all larger than the 10V MM at the studied reaction temperatures, but the differences are slight.



**Figure 10.** The conversion rate of 10V IM and 10V MM at different reaction temperatures.

### 3. Materials and Methods

In this section, the preparation methods of the oxygen carriers are described, followed by a short description of the characterization techniques and the procedures for the thermogravimetric analysis and reactivity performance tests.

#### 3.1. Oxygen Carrier Synthesis

##### 3.1.1. Impregnation Method

Four oxygen carriers with different V loadings were prepared with the impregnation method (5 wt.%, 10 wt.%, 15 wt.% and 20 wt.% labeled as 5V IM, 10V IM, 15V IM and 20V IM, respectively). In the incipient wetness impregnation method, the active phase precursor (ammonium metavanadate, Sigma-Aldrich, ACS reagent, >99%) was first dissolved in distilled water, and subsequently  $\text{Al}_2\text{O}_3$  (Sigma-Aldrich, Zwijndrecht, The Netherlands) was added to the solvent which was uniformly mixed. After that, the water bath mixer was used to stir the mixture at 80 °C to evaporate the water. After most of water was evaporated, the residue was calcined in the oven under air conditions: first at 450 °C for 4 h to decompose the precursor, and then at 850 °C for another 4 h to increase the mechanical strength of the oxygen carrier. After the calcination, the oxygen carrier precursor was obtained and finally a mortar, pestle and sieves were used to get the oxygen carrier particles to the desired size (75~105  $\mu\text{m}$ ). The preparation procedure of impregnation method is shown in Figure 11.

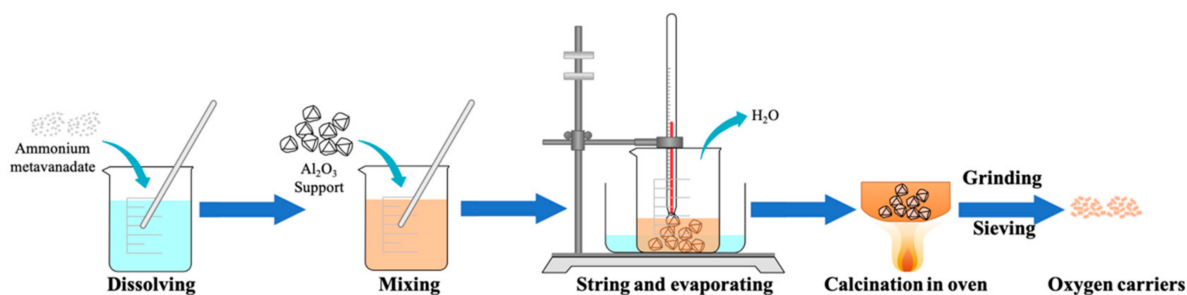


**Figure 11.** The preparation procedure of impregnation method.

##### 3.1.2. Mechanical Mixing Method

Four oxygen carriers with different V loading (5 wt.%, 10 wt.%, 15 wt.% and 20 wt.%, named 5V MM, 10V MM, 15V MM and 20V MM, respectively) were prepared by mechanical mixing. In this procedure, ammonium metavanadate (Sigma-Aldrich, Zwijndrecht, The Netherlands, ACS reagent, >99%) was first calcined in air at 450 °C for 4 h to obtain the

crystalline  $V_2O_5$ . Then, a planetary centrifugal mixer (ARE-250, Thinky) was used to mix  $V_2O_5$  and  $Al_2O_3$  uniformly for 30 min. Finally, the mixture was calcined in air with the same conditions and procedure as for the impregnation method, and oxygen carrier particles were obtained following the same procedures (grinding and sieving) as for the impregnation method. The preparation procedure of mechanical mixing method is shown in Figure 12.

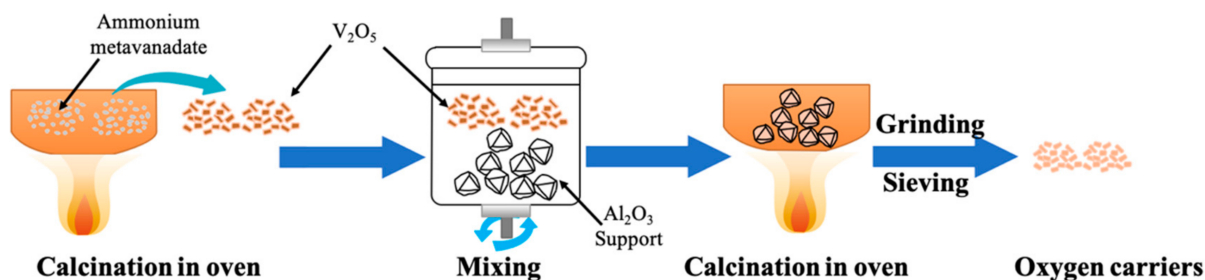


**Figure 12.** The preparation procedure of mechanical mixing method.

### 3.2. Surface Area Measurements

A Micromeritics TriStar II was used to measure the surface area of the as-prepared oxygen carriers at  $-196$  °C. Before measurement, all the as-prepared oxygen carriers were degassed under  $N_2$  at  $100$  °C for 4 h. Based on the Brunauer-Emmett-Teller (BET) theory, the surface areas of oxygen carriers were calculated from the  $N_2$  isothermal adsorption.

### 3.3. XRD Characterization

Powder X-ray Diffraction (XRD) characterizations were performed to identify the crystal phase in the as-prepared oxygen carriers. The characterizations were performed with a Rigaku MiniFlex 600 with a  $Cu-K\alpha$  radiation and diffractometer was operated at 40 kV and 15 mA. The scanning range and rate of XRD pattern were  $10^\circ$  to  $90^\circ$  ( $2\theta$ ) and  $0.4^\circ/\text{min}$ .

### 3.4. SEM-EDX Analysis

The particle structure and surface morphology of the oxygen carriers was obtained using a Scanning Electron Microscope on a Phenom Prox. The same system was also used to obtain the elements distribution of the oxygen carrier using Energy Dispersive Spectrometry (EDX).

### 3.5. Thermogravimetric Analysis

The redox properties of the as-prepared oxygen carriers were investigated by  $H_2$ -TPR,  $O_2$ -TPO and isothermal redox cycles using a thermogravimetric analysis (TGA) system. Before the measurement, 0.05 g of the prepared oxygen carrier was loaded into the cup of the TGA system. After that, the micro reactor was heated from room temperature to  $850$  °C with a rate of  $10$  °C/min in air to keep the active sites of the oxygen carrier oxidized and then cooled down to room temperature. During the TGA experiment, the total gas flows were all set to 500 mL/min.

For  $H_2$ -TPR, the micro reactor was heated from room temperature to  $700$  °C with a  $10$  °C/min heating rate under a 10%  $H_2/90\%$   $N_2$  condition and kept at the final temperature for 30 min to fully reduce the oxygen carrier. Subsequently, the micro reactor was cooled down to room temperature under a 100%  $N_2$  flow. Finally, the micro reactor was re-heated to  $850$  °C using a  $10$  °C/min heating rate with a 10% air/90%  $N_2$  flow which was kept for another 30 min for the  $O_2$ -TPO experiment.

For isothermal redox cycles, the micro reactor was first heated to  $615$  °C with a  $10$  °C/min heating rate in a 100%  $N_2$  flow. Then, the gas flow was switched to 10%  $H_2/90\%$

N<sub>2</sub> and held for 60 min for the reduction reaction. After that, the temperature of micro reactor was changed to 435 °C under 100% N<sub>2</sub> conditions, and subsequently the gas flow was switched to 100% air flow, which was kept for 60 min for the oxidation reaction. Before and after the reduction and oxidation reactions, a 100% N<sub>2</sub> flow was used to purge the micro reactor for 5 min.

### 3.6. Reactivity Performance Test

The reactivity of the prepared oxygen carriers was quantified in a fixed bed reactor (14 mm outer diameter and 10 mm inner diameter) system. The oxygen carrier (1.0 g) was loaded in the center of the fixed bed reactor and 16 mesh quartz particles were loaded up- and downstream of the oxygen carrier bed. The reactor was heated by a temperature-controlled tube oven and two thermocouples were used to control and measure the temperature in the reactor. The feed gas flow rate for the reactor was controlled by mass flow controllers, and during these tests the total gas flow rates were all set to 40 mL/min.

For the ODHP reaction, a feed gas consisting of C<sub>3</sub>H<sub>8</sub> and N<sub>2</sub> (C<sub>3</sub>H<sub>8</sub>/N<sub>2</sub> volume ratio = 1:1) was fed to reactor. For the oxygen carrier re-oxidation reaction, 100% air was fed to the reactor to re-oxidize the reduced oxygen carrier. Before and after the ODHP reaction and re-oxidation reaction cycles, a N<sub>2</sub> purge was used for 10 min. The exhaust gas was analyzed by an on-line gas chromatography system (Agilent 490 Micro GC system) with TCD (Thermal conductivity detector) gas detectors.

For the ODHP reaction, the propane conversion and product selectivity were calculated as follows:

$$\text{C}_3\text{H}_8 \text{ conversion} = (\text{C}_3\text{H}_8 \text{ in} - \text{C}_3\text{H}_8 \text{ out}) / \text{C}_3\text{H}_8 \text{ in} \times 100\% \quad (4)$$

$$\text{C}_3\text{H}_6 \text{ selectivity} = \text{C}_3\text{H}_6 \text{ out} / (\text{C}_3\text{H}_8 \text{ in} - \text{C}_3\text{H}_8 \text{ out}) \times 100\% \quad (5)$$

$$\text{CO}_x \text{ selectivity} = 3 \times \text{CO}_x \text{ out} / (\text{C}_3\text{H}_8 \text{ in} - \text{C}_3\text{H}_8 \text{ out}) \times 100\% \quad (6)$$

$$\text{C}_3\text{H}_6 \text{ yield} = \text{C}_3\text{H}_6 \text{ out} / \text{C}_3\text{H}_8 \text{ in} \times 100\% \quad (7)$$

where C<sub>3</sub>H<sub>8 in</sub> and C<sub>3</sub>H<sub>8 out</sub> are the molar flow rate of propane fed to and exiting from the reactor, respectively, and C<sub>3</sub>H<sub>6 out</sub> and CO<sub>x out</sub> are the propylene and CO<sub>x</sub> molar flow rates exiting from the reactor.

For the oxygen carrier re-oxidation reaction, the oxygen carrier conversion and conversion rate of the oxygen carrier are calculated using the following equations:

$$\alpha = \frac{\int_0^t (Q'_{\text{out}} - Q_{\text{out}}) dt}{\int_0^{t_{\text{total}}} (Q'_{\text{out}} - Q_{\text{out}}) dt} \quad (8)$$

$$d\alpha/dt = \alpha/t \quad (9)$$

where Q'<sub>out</sub> and Q<sub>out</sub> are the oxygen content in the gas stream leaving the reactor during the oxygen carrier re-oxidation without reaction and with reaction, respectively (mL/min); α is the oxygen conversion; t is the reaction time (min); and t<sub>total</sub> is the time for the complete conversion of the reduced oxygen carrier (min).

## 4. Conclusions

The influences of different V loadings and preparation methods, viz. impregnation and mechanical mixing, on the properties and reactivity performance of V-based oxygen carriers have been investigated for CL-ODHP. It was observed that the surface areas of the prepared V-based oxygen carriers decrease with increasing V loadings, because the VO<sub>x</sub> species enter and block the pore channels of the Al<sub>2</sub>O<sub>3</sub> support during the preparation. At low V loadings (5 wt.% and 10 wt.%), the VO<sub>x</sub> species can be distributed well over the support, but when the V loading is higher than 10 wt.%, the VO<sub>x</sub> species become more aggregated. Moreover, it was found that the VO<sub>x</sub> species on the oxygen carriers prepared by impregnation are distributed better on the support compared to mechanical mixing.

All the prepared V-based oxygen carriers showed a stable redox performance, where the reduction and oxidation temperatures and oxygen transport capacity increase for oxygen carriers with a higher V loading. At a high V loading, the oxygen carrier capacity of the V-based oxygen carriers prepared by the mechanical mixing method is larger than those prepared by the impregnation method. With increased V loading, the propane conversion and CO<sub>x</sub> selectivity decrease, while the propylene selectivity increase. The propylene yield reaches its maximum when the V loading is around 10 wt.%. With higher V loadings, the amount of oxygen needed by the reduced oxygen carrier for the re-oxidation reaction increases, while the reaction rate decreases, where the V-based oxygen carriers prepared by impregnation exhibited a better performance for ODHP and re-oxidation reactions than oxygen carriers prepared by mechanical mixing. For the re-oxidation reaction, a higher reaction temperature can promote the oxygen adsorption, but for the ODHP reaction, the higher reaction temperature promotes the occurrence of undesired reactions, which decreases the propylene selectivity. Therefore, the V-based oxygen carriers show potential for CL-ODHP and their reactivity performance can be improved by controlling preparation method and loading.

**Author Contributions:** Conceptualization, T.W., Q.Y. and M.v.S.A.; methodology, T.W.; formal analysis, T.W., Q.Y., K.W. and M.v.S.A.; investigation, T.W.; writing—original draft preparation, T.W.; supervision, Q.Y. and M.v.S.A.; funding acquisition, Q.Y. and K.W.; project administration, M.v.S.A.; writing—review and editing, K.W. and M.v.S.A. All authors have read and agreed to the published version of the manuscript.

**Funding:** This research was funded by China Scholarship Council, grant number CSC201806080086, National Natural Science Foundation of China, grant number 51604078 and Fundamental Research Funds for the Central Universities, grant number N182504011.

**Institutional Review Board Statement:** Not applicable.

**Informed Consent Statement:** Not applicable.

**Data Availability Statement:** The data used during the study appear in this submitted article.

**Conflicts of Interest:** The authors declare no conflict of interest.

## References

1. Liu, G.; Zhao, Z.-J.; Wu, T.; Zeng, L.; Gong, J. Nature of the active sites of VO<sub>x</sub>/Al<sub>2</sub>O<sub>3</sub> catalysts for propane dehydrogenation. *ACS Catal.* **2016**, *6*, 5207–5214. [\[CrossRef\]](#)
2. Makishima, A. *Biochemistry for Materials Science*; Elsevier: Amsterdam, The Netherlands, 2019; pp. 3–32.
3. Mitran, G.; Ahmed, R.; Iro, E.; Hajimirzaee, S.; Hodgson, S.; Urdã, A.; Olea, M.; Marcu, I.-C. Propane oxidative dehydrogenation over VO<sub>x</sub>/SBA-15 catalysts. *Catal. Today* **2018**, *306*, 260–267. [\[CrossRef\]](#)
4. Nawaz, Z. Light alkane dehydrogenation to light olefin technologies: A comprehensive review. *Rev. Chem. Eng.* **2015**, *31*, 413–436. [\[CrossRef\]](#)
5. Daniell, W.; Ponchel, A.; Kuba, S.; Anderle, F.; Weingand, T.; Gregory, D.H.; Knözinger, H. Characterization and catalytic behavior of VO<sub>x</sub>-CeO<sub>2</sub> catalysts for the oxidative dehydrogenation of propane. *Top. Catal.* **2002**, *20*, 65–74. [\[CrossRef\]](#)
6. Cavani, F.; Ballarini, N.; Cericola, A. Oxidative dehydrogenation of ethane and propane: How far from commercial implementation? *Catal. Today* **2007**, *127*, 113–131. [\[CrossRef\]](#)
7. Hu, P.; Lang, W.-Z.; Yan, X.; Chen, X.-F.; Guo, Y.-J. Vanadium-Doped porous silica materials with high catalytic activity and stability for propane dehydrogenation reaction. *Appl. Catal. A Gen.* **2018**, *553*, 65–73. [\[CrossRef\]](#)
8. Ovsitser, O.; Schomaecker, R.; Kondratenko, E.V.; Wolfram, T.; Trunschke, A. Highly selective and stable propane dehydrogenation to propene over dispersed VO<sub>x</sub>-species under oxygen-free and oxygen-lean conditions. *Catal. Today* **2012**, *192*, 16–19. [\[CrossRef\]](#)
9. Sun, L.; Chai, Y.; Dai, W.; Wu, G.; Guan, N.; Li, L. Oxidative dehydrogenation of propane over Pt-Sn/Si-Beta catalysts: Key role of Pt-Sn interaction. *Catal. Sci. Technol.* **2018**, *8*, 3044–3051. [\[CrossRef\]](#)
10. Neal, L.M.; Yusuf, S.; Sofranko, J.A.; Li, F. Oxidative dehydrogenation of ethane: A chemical looping approach. *Energy Technol.* **2016**, *4*, 1200–1208. [\[CrossRef\]](#)
11. Yusuf, S.; Haribal, V.; Jackson, D.; Neal, L.; Li, F. Mixed iron-manganese oxides as redox catalysts for chemical looping—Oxidative dehydrogenation of ethane with tailorable heat of reactions. *Appl. Catal. B Environ.* **2019**, *257*, 117885. [\[CrossRef\]](#)
12. Baek, J.; Yun, H.J.; Yun, D.; Choi, Y.; Yi, J. Preparation of highly dispersed chromium oxide catalysts supported on Mesoporous Silica for the oxidative dehydrogenation of propane using CO<sub>2</sub>: Insight into the nature of catalytically active chromium sites. *ACS Catal.* **2012**, *2*, 1893–1903. [\[CrossRef\]](#)

13. Wang, S.; Zhu, Z.H. Catalytic conversion of alkanes to olefins by carbon dioxide oxidative dehydrogenation—A review. *Energy Fuels* **2004**, *18*, 1126–1139. [[CrossRef](#)]
14. Wu, T.; Yu, Q.; Qin, Q. Energy analysis of chemical looping oxidative dehydrogenation of propane. *Pet. Sci. Technol.* **2018**, *36*, 266–272. [[CrossRef](#)]
15. De Graaf, E.A.; Rothenberg, G.; Kooyman, P.J.; Andreini, A.; Blik, A. Pt<sub>0.02</sub>Sn<sub>0.003</sub>Mg<sub>0.06</sub> on  $\gamma$ -Alumina: A stable catalyst for oxidative dehydrogenation of ethane. *Appl. Catal. A Gen.* **2005**, *278*, 187–194. [[CrossRef](#)]
16. Ballarini, N.; Cavani, F.; Cericola, A.; Cortelli, C.; Ferrari, M.; Trifirò, F.; Capannelli, G.; Comite, A.; Catani, R.; Cornaro, U. Supported vanadium oxide-based catalysts for the oxidehydrogenation of propane under cyclic conditions. *Catal. Today* **2004**, *91–92*, 99–104. [[CrossRef](#)]
17. Neal, L.; Yusuf, S.; Sofranko, J.; Li, F. Alkali-Doped manganese oxides as redox catalysts for oxidative dehydrogenation of ethane. In Proceedings of the Abstract of Papers of the American Chemical Society, Washington, DC, USA, 16 August 2015; p. 1155.
18. Wang, Y.; Xie, S.; Yue, B.; Feng, S.; He, H. Oxidative dehydrogenation of propane to propene over mesoporous alu-mina-supported vanadium oxide catalyst. *Chin. J. Catal. Chin. Version* **2010**, *31*, 1054–1060. [[CrossRef](#)]
19. Imtiaz, Q.; Hosseini, D.; Müller, C.R. Review of oxygen carriers for chemical looping with oxygen uncoupling (CLOU): Thermodynamics, material development, and synthesis. *Energy Technol.* **2013**, *1*, 633–647. [[CrossRef](#)]
20. Löfberg, A.; Giornelli, T.; Paul, S.; Bordes-Richard, E. Catalytic coatings for structured supports and reactors: VO<sub>x</sub>/TiO<sub>2</sub> catalyst coated on stainless steel in the oxidative dehydrogenation of propane. *Appl. Catal. A Gen.* **2011**, *391*, 43–51. [[CrossRef](#)]
21. Alexopoulos, K.; Reyniers, M.-F.; Marin, G.B. Reaction path analysis of propane selective oxidation over V<sub>2</sub>O<sub>5</sub> and V<sub>2</sub>O<sub>5</sub>/TiO<sub>2</sub>. *J. Catal.* **2012**, *289*, 127–139. [[CrossRef](#)]
22. Medrano, J.A.; Hamers, H.P.; Williams, G.; Van Sint Annaland, M.; Gallucci, F. NiO/CaAl<sub>2</sub>O<sub>4</sub> as active oxygen carrier for low temperature chemical looping applications. *Appl. Energy* **2015**, *158*, 86–96. [[CrossRef](#)]
23. Wang, K.; Yu, Q. Long-Lasting investigation of the Cu-Based oxygen carrier particles in chemical looping air separation. *Powder Technol.* **2019**, *343*, 40–48. [[CrossRef](#)]
24. Rydén, M.; Jing, D.; Källén, M.; Leion, H.; Lyngfelt, A.; Mattisson, T. CuO-Based oxygen-carrier particles for chemical-looping with oxygen uncoupling—Experiments in batch reactor and in continuous operation. *Ind. Eng. Chem. Res.* **2014**, *53*, 6255–6267. [[CrossRef](#)]
25. Zhao, H.; Mei, D.; Ma, J.; Zheng, C. Comparison of preparation methods for iron-alumina oxygen carrier and its reduction kinetics with hydrogen in chemical looping combustion. *Asia Pac. J. Chem. Eng.* **2014**, *9*, 610–622. [[CrossRef](#)]
26. Zhao, H.; Liu, L.; Wang, B.; Xu, D.; Jiang, L.; Zheng, C. Sol–Gel-Derived NiO/NiAl<sub>2</sub>O<sub>4</sub> oxygen carriers for chemical-looping combustion by coal char. *Energy Fuels* **2008**, *22*, 898–905. [[CrossRef](#)]
27. Hossain, M.M.; Lasa, H.I. De reactivity and stability of Co-Ni/Al<sub>2</sub>O<sub>3</sub> oxygen carrier in multicycle CLC. *AIChE J.* **2007**, *53*, 1817–1829. [[CrossRef](#)]
28. Wang, S.; Wang, G.; Jiang, F.; Luo, M.; Li, H. Chemical looping combustion of coke oven gas by using Fe<sub>2</sub>O<sub>3</sub>/CuO with MgAl<sub>2</sub>O<sub>4</sub> as oxygen carrier. *Energy Environ. Sci.* **2010**, *3*, 1353–1360. [[CrossRef](#)]
29. Zhu, X.; Wei, Y.; Wang, H.; Li, K. Ce–Fe oxygen carriers for chemical-looping steam methane reforming. *Int. J. Hydrog. Energy* **2013**, *38*, 4492–4501. [[CrossRef](#)]
30. Tang, M.; Xu, L.; Fan, M. Progress in oxygen carrier development of methane-based chemical-looping reforming: A review. *Appl. Energy* **2015**, *151*, 143–156. [[CrossRef](#)]
31. Cao, Y.; Sit, S.P.; Pan, W.-P. Preparation and characterization of lanthanum-promoted copper-based oxygen carriers for chemical looping combustion process. *Aerosol Air Qual. Res.* **2014**, *14*, 572–584. [[CrossRef](#)]
32. Bulánek, R.; Čičmanec, P.; Sheng-Yang, H.; Knotek, P.; Čapek, L.; Setnička, M. Effect of preparation method on nature and distribution of vanadium species in vanadium-based hexagonal Mesoporous Silica catalysts: Impact on catalytic behavior in propane ODH. *Appl. Catal. A Gen.* **2012**, *415*, 29–39. [[CrossRef](#)]
33. Karakoulia, S.A.; Triantafyllidis, K.S.; Tsilomelekis, G.; Boghosian, S.; Lemonidou, A.A. Propane oxidative dehydrogenation over vanadia catalysts supported on Mesoporous Silicas with varying pore structure and size. *Catal. Today* **2009**, *141*, 245–253. [[CrossRef](#)]
34. Johansson, M.; Mattisson, T.; Lyngfelt, A. Use of NiO/NiAl<sub>2</sub>O<sub>4</sub> particles in a 10 KW chemical-looping combustor. *Ind. Eng. Chem. Res.* **2006**, *45*, 5911–5919. [[CrossRef](#)]
35. Lancee, R.J.; Dugulan, A.I.; Thüne, P.C.; Veringa, H.J.; Niemantsverdriet, J.W.; Fredriksson, H.O.A. Chemical looping capabilities of olivine, used as a catalyst in indirect biomass gasification. *Appl. Catal. B Environ.* **2014**, *145*, 216–222. [[CrossRef](#)]
36. Galinsky, N.L.; Shafiefarhood, A.; Chen, Y.; Neal, L.; Li, F. Effect of support on redox stability of iron oxide for chemical looping conversion of methane. *Appl. Catal. B Environ.* **2015**, *164*, 371–379. [[CrossRef](#)]
37. Qiao, A.; Kalevaru, V.N.; Radnik, J.; Düvel, A.; Heitjans, P.; Kumar, A.S.H.; Prasad, P.S.S.; Lingaiah, N.; Martin, A. Oxidative dehydrogenation of ethane to ethylene over V<sub>2</sub>O<sub>5</sub>/Al<sub>2</sub>O<sub>3</sub> catalysts: Effect of source of alumina on the catalytic performance. *Ind. Eng. Chem. Res.* **2014**, *53*, 18711–18721. [[CrossRef](#)]
38. Taylor, M.N.; Carley, A.F.; Davies, T.E.; Taylor, S.H. The oxidative dehydrogenation of propane using vanadium oxide supported on Nanocrystalline Ceria. *Top. Catal.* **2009**, *52*, 1660–1668. [[CrossRef](#)]
39. Schwarz, O.; Habel, D.; Ovsitser, O.; Kondratenko, E.V.; Hess, C.; Schomäcker, R.; Schubert, H. Impact of preparation method on physico-chemical and catalytic properties of VO<sub>x</sub>/ $\gamma$ -Al<sub>2</sub>O<sub>3</sub> materials. *J. Mol. Catal. A Chem.* **2008**, *293*, 45–52. [[CrossRef](#)]

40. Chen, S.; Qin, Z.; Xu, X.; Wang, J. Structure and properties of the alumina-supported vanadia catalysts for ethylbenzene dehydrogenation in the presence of carbon dioxide. *Appl. Catal. A Gen.* **2006**, *302*, 185–192. [[CrossRef](#)]
41. Garcia, E.M.; Sanchez, M.D.; Tonetto, G.; Volpe, M.A. Preparation of USY Zeolite VO<sub>x</sub> supported catalysts from V(AcAc)<sub>3</sub> and NH<sub>4</sub>VO<sub>3</sub>. Catalytic properties for the dehydrogenation of n-butane in oxygen-free atmosphere. *J. Colloid Interface Sci.* **2005**, *292*, 179–185. [[CrossRef](#)]
42. Rostom, S.; De Lasa, H. High propylene selectivity via propane oxidative dehydrogenation using a novel fluidizable catalyst: Kinetic modeling. *Ind. Eng. Chem. Res.* **2018**, *57*, 10251–10260. [[CrossRef](#)]
43. Al-Ghamdi, S.; Moreira, J.; De Lasa, H. Kinetic modeling of propane oxidative dehydrogenation over VO<sub>x</sub>/γ-Al<sub>2</sub>O<sub>3</sub> catalysts in the Chemical Reactor Engineering Center Riser Reactor Simulator. *Ind. Eng. Chem. Res.* **2014**, *53*, 15317–15332. [[CrossRef](#)]
44. Al-Ghamdi, S.A.; De Lasa, H.I. Propylene production via propane oxidative dehydrogenation over VO<sub>x</sub>/γ-Al<sub>2</sub>O<sub>3</sub> catalyst. *Fuel* **2014**, *128*, 120–140. [[CrossRef](#)]
45. Fukudome, K.; Ikenaga, N.; Miyake, T.; Suzuki, T. Oxidative dehydrogenation of alkanes over vanadium oxide prepared with V(t-BuO)<sub>3</sub>O and Si(OEt)<sub>4</sub> in the presence of polyethyleneglycol. *Catal. Today* **2013**, *203*, 10–16. [[CrossRef](#)]
46. Rostom, S.; De Lasa, H. Propane oxidative dehydrogenation on vanadium-based catalysts under oxygen-free atmospheres. *Catalysts* **2020**, *10*, 418. [[CrossRef](#)]
47. Xie, Q.; Zhang, H.; Kang, J.; Cheng, J.; Zhang, Q.; Wang, Y. Oxidative dehydrogenation of propane to propylene in the presence of HCl catalyzed by CeO<sub>2</sub> and NiO-Modified CeO<sub>2</sub> nanocrystals. *ACS Catal.* **2018**, *8*, 4902–4916. [[CrossRef](#)]
48. Carrero, C.A.; Schloegl, R.; Wachs, I.E.; Schomaecker, R. Critical literature review of the kinetics for the oxidative dehydrogenation of propane over well-defined supported vanadium oxide catalysts. *ACS Catal.* **2014**, *4*, 3357–3380. [[CrossRef](#)]
49. Fattahi, M.; Kazemeini, M.; Khorasheh, F.; Rashidi, A. Kinetic modeling of oxidative dehydrogenation of propane (ODHP) over a vanadium–graphene catalyst: Application of the DOE and ANN methodologies. *J. Ind. Eng. Chem.* **2014**, *20*, 2236–2247. [[CrossRef](#)]
50. Rostom, S.; De Lasa, H.I. Propane oxidative dehydrogenation using consecutive feed injections and fluidizable VO<sub>x</sub>/γ-Al<sub>2</sub>O<sub>3</sub> and VO<sub>x</sub>/ZrO<sub>2</sub>-γ-Al<sub>2</sub>O<sub>3</sub> catalysts. *Ind. Eng. Chem. Res.* **2017**, *56*, 13109–13124. [[CrossRef](#)]